crystals

Concept Paper

Ti:Sa Crystal Geometry Variation vs. Final Amplifiers of CPA Laser Systems Parameters

Vladimir Chvykov

Center for Extreme Ultraviolet Science and Technology, Colorado State University, Fort Collins, CO 80523, USA; vladimir.chvykov@colostate.edu

Abstract: In this paper, the different Ti:Sapphire crystal configurations of the final amplifiers, depending on the Chirped Pulse Amplification laser system parameters, such as the repetition rates and pulse energy, are discussed. Restrictions placed on the final Ti:Sa amplifiers with a high repetition rate are discussed. The repetition rate of these systems is limited due to the crystal overheating, which leads to stress fracturing or significant beam distortion. The heating density threshold leading to stress fracturing was calculated and taken as the limit of the upper level of the possible pump average power. On the basis of these calculations, the highest repetition rates and corresponding thermolens focal distances were estimated for conventional crystal geometry of the most suitable thicknesses. It was demonstrated that conventional crystal shapes, such as a thin disc, can be used for systems with repetition rates below a few hundred Hz if several Joules of the output pulse energy are required. The rectangular thin crystal plate geometry was more suitable for Ti:Sa amplifiers with repetition rates above 1 kHz. Finally, the parameters of rectangular thin crystal plate Ti:Sa laser amplifier with an output energy above 3 J per pulse for a laser system with more than 100 TW pulse power and 1 kHz repetition rates are presented.

Keywords: Ti:Sa amplifiers; CPA laser systems; high power laser systems; Ti:Sa crystals properties

Citation: Chvykov, V. Ti:Sa Crystal Geometry Variation vs. Final Amplifiers of CPA Laser Systems Parameters. *Crystals* **2022**, *12*, 1127. https://doi.org/10.3390/cryst12081127

Academic Editor: Ludmila Isaenko

Received: 30 July 2022
Accepted: 9 August 2022
Published: 11 August 2022

1. Introduction

Recent laser technology progress is related to the development of the ultra-high power of the extremely short pulse duration laser systems. The Chirped Pulse Amplification (CPA) technique [1,2] in combination with the unique properties of a Ti:Sapphire (Ti:Sa) crystal [3] and the extraction during pumping (EDP) method [4,5] allows for 400 J [6] to be concentrated into the very small volume of a few cubic microns, which results in an energy density of 10^{13}–10^{14} J/cm^3 and a light pulse intensity up to 10^{23} W/cm^2 [7]. These achievements allow us to investigate the physics of plasma and vacuum with new parameters [8] and suggest the way forward for very efficient methods of elementary particle acceleration and secondary light source production, such as a gamma and X-ray, which can be applied in many areas of science and industry [9]. Although scientific research permits the usage of single-shot or low-repetition-rate (RR) laser systems in many experiments, industrial applications require a significant increase in the RR. However, the RR of the existing laser systems discussed above is low, typically limited by a few Hz or less.

TD geometry of the laser amplifiers active media, such as Yb:YAG, was used for effective heat dissipation and resulted in 100 kW output power in CW regimes [10] and up to several Joules per pulse and high average power in a master oscillator—a power amplifier (MOPA) system [11,12]. In the thin-disc (TD) amplifiers, the heat is extracted through the largest face of the crystal for efficient and uniform cooling, in contrast to the conventional side surface heat extraction. The very high thermal conductivity Ti:Sa crystal in combination with TD technology allows for this effect to be increased, preventing the overheating of the laser crystals and, thus, eliminating the beam thermal distortions and possible crystal damage even for an extremely high average power operation regime [13,14].

Nevertheless, the TD crystal shape is not the only possible configuration for the final amplifier of the laser systems, which changes with their output parameters. Further in the paper, the maximal possible pump fluence of the amplifier crystal depending on the RR will be shown, which consequently influences the choice of the crystal shape.

The average power of the laser system can be increased by two different ways, which require different approaches. Raising the pulse energy can be achieved through increasing the fluence and the enlargement of the TD diameter. In the second case, the RR increases, keeping a fixed pulse energy. The TD and the seed beam diameter enlargement will lead to the seed fluence reduction and consequently to an inefficient extraction of the energy accumulated in the amplifier. A low seed gain per pass requires a significant increase in the number of passes. Furthermore, the large aperture of the optical elements increases the distances between the mirrors and the crystal and, consequently, the total time of the seed passing through the amplifier. Taking into consideration the shortening of the lifetime of the upper laser level from 3.2 μs down to 100 ns due the amplified spontaneous emission (ASE), the utilization of the TD type of crystal configuration becomes problematic in this case, and changing the crystal geometry is required.

Recently, a cross thin slab (XTS) configuration was suggested to mitigate the inconsistency between the efficiency of the energy extraction and the heat removal [15]. The heat was extracted through the top and bottom largest surfaces of the slab, and the different passes of the seed were run through the narrow crystal side surface. The seed and pump beams were crossed in the crystal of the amplifier, in contrast to the slab configuration [16,17], where the pump and seed beams are passed into the crystal through the same side. XTS geometry allowed the spatial separation of the pump and seed beams, resulting in a more compact package and easier alignment; besides, the crystal damage threshold can be reduced by allowing an independent selection of the crystal surfaces for the pump. The Ti:Sa amplifier with XTS geometry was successfully realized in [18], demonstrating 30 mJ with an RR up to 1 kHz.

Nevertheless, the energy scaling is limited for XTS configuration due to the necessity of increasing the beam diameter and, consequently, the crystal thickness, which in turn limits the heat extraction. Furthermore, the rising of the RR with the fixed energy leads to significant thermolens developing due to long seed passes in the pumped area of the crystal. These obstacles can be resolved by using the rectangular thin plate as the crystal shape (RTCP), which allows a notable enlargement of the heat extraction surface and pump beam diameter, keeping the seed small enough for it to hold a fluence near the saturation level. The crystal aperture is filled by directing the different seed passes through the neighbor area of the crystal [3], as is done for XTS geometry. In this paper, Ti:Sa crystal shape variation depending on the final amplifiers parameters of CPA laser systems was detailed. Furthermore, the estimation of the possibility of building a Ti:Sa amplifier for a laser system with an output peak power of 100 s TW and a repetition rate above 1 kHz was carried out.

2. Limits of Crystal Heating and Thermal Lensing

CPA laser systems demonstrate an ability to produce a very high peak pulse power; however, the increase in the repetition rate leads to significant overheating of the amplifier's crystals. Thus, we started this investigation with the estimation of the maximal possible Ti:Sa crystal heating that can be accepted.

One of the conventional optical schemes of the multipass amplifier is presented in Figure 1a. Here, the seed beam of each pass goes through the almost full aperture of the laser crystal, overlapping with the pump beams. For further appraisal of the calculations, the squared-thin-plate (STP) configuration of the amplifier Ti:Sa crystal was used (Figure 1b). The heat density calculation in this configuration is valid for all crystal shapes discussed above (TD, XTS, and RTCP). In Figure 1b, the violet color shows the crystal area engaged by the seed beam, and the green one shows the pump beam. The crystal is cooled by the room temperature coolant flow directly connected to both XY is the largest surface.

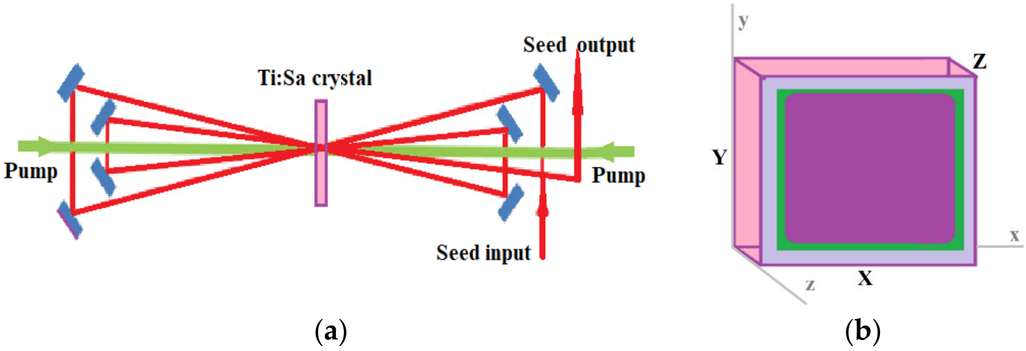

Figure 1. Ti:Sa crystal geometry for an estimation: (**a**) optical scheme; (**b**) squared thin plate of Ti:Sa crystal.

The highest power of the laser crystal pumping is restricted by the stress fracture limit σ_{max}, which determines the maximal heating transmitted by the pump power before the crystal cracks. The estimation of this factor [19] can be achieved with the formula:

$$\sigma_{max} = \frac{R}{M}, \tag{1}$$

where M is the material parameter $M = \frac{K(1-\nu)}{aE}$.

Here, for sapphire, R is the thermal shock parameter (100 W/cm) [20], K is the thermal conductivity near the room temperature (33 W/mK), ν is the Poisson ratio (0.29), a is the expansion coefficient (5×10^{-6} K^{-1}), and E is the Yong modulus (335 GPa) [21]. Thus, σ_{max} can be estimated as ~10^5 psi. For the plate configuration, the generated heat density (Q) producing this stress can be calculated by the next formula:

$$Q = \frac{12M\sigma_{max}}{Z^2}. \tag{2}$$

Combining Formula (1) and (2) we can obtain

$$Q = \frac{12R}{Z^2}\ [\mathrm{W/cm^3}], \tag{3}$$

where Z is the crystal thickness. The choice of Z for the thin-plate or slab crystal geometry relates to a used material. For a Ti:Sa crystal, a trade between the reasonable pump absorption per pass and the effective heat extraction can be achieved. The range of 2–6 mm was considered, taking into account the very high thermoconductivity of sapphire and the conventional doping concentration of Ti^{3+} ions in the crystal at about 0.25%. The heating density levels starting from the stress fracture limit (blue) and two (orange), four (gray), and six (green) times below this limit on the crystal thickness is shown in Figure 2. The recent two curves of heat density are presented as more realistic for the amplifier operation.

As seen from the curves, the limited heat density became smaller with the growth of the crystal thickness, which indicates the restriction on the seed beam diameter and, in turn, on the pulse energy in the case of XTS geometry. This led to the necessity of a change in the crystal shape for further energy scaling.

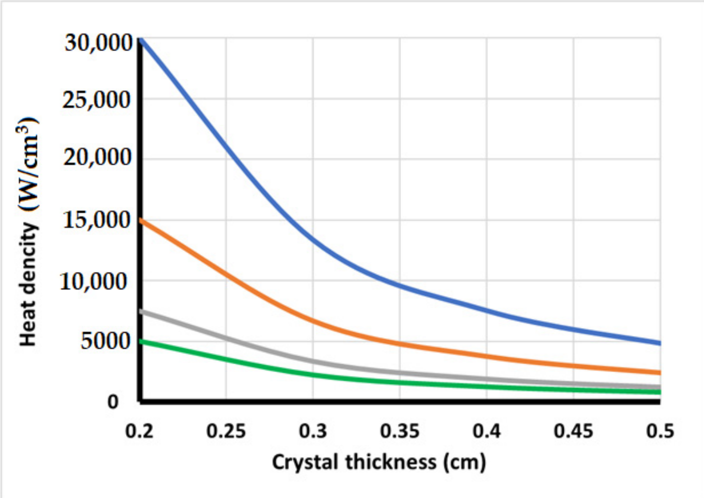

Figure 2. Heating density levels in W/cm^3, the stress fracture limit (blue), two (orange), four (gray), and six (green) times below this limit on the crystal thickness in cm.

The amplifier optical scheme design, among others, requires the evaluation of the beam distortion due to the thermolens developing as a result of the pump heating for the crystal thickness at the maximal temperature possible for the amplifier operation. In [18], the thermolens of focal distance of 60 cm was measured for an XTS Ti:Sa crystal of $10 \times 10 \times 4$ mm and pumped by 100 mJ with a temperature difference of 20 K. This result demonstrates the problematic use of this type of amplifier when temperature differences increase up to 100 K. The thermolens estimation requires the calculation of the temperature distribution within the crystal. We can assume the uniform distribution of the heat energy through the *XY* surface of the crystal when the pump beams have a flat-top cross-section energy distribution. A one-dimensional temperature spreading along the z axis in the crystal is described analytically by the steady-state heat conduction equation.

$$\frac{\mathrm{D}^2\mathrm{T}}{\mathrm{dz}^2} = -\frac{Q}{K} \tag{4}$$

where T is temperature and z is the thickness coordinate. The solution to this equation shows the dependence of the temperature difference ΔT on the z-point.

$$\Delta T(z) = -\frac{Q}{2K}z^2 + \frac{Q}{2K}Zz \tag{5}$$

here, Z is a total crystal thickness, K is the thermal conductivity, and Q is the heat density.

Formula (5) can be converted for temperature differences between the surface and center of the crystal ($z = Z/2$), where the temperature is maximal, in the form:

$$\Delta T = \frac{Q}{8K}Z^2. \tag{6}$$

Replacing formula (6) Q from (3), one finds that the crystal center temperature was independent of the crystal thickness. For example, for the Ti:Sa crystal, the heating density was six times below the stress fracture limit $\Delta T = R/4K$. The thermal conductivity was taken as the constant (30 W/mK) and equaled the average value of the range between the room temperature 20 °C (33 W/mK) and maximal acceptable temperature of the operation 100 °C (25 W/mK). Thus, using the last formula, one can obtain the realistic temperature difference between the cooling surface and the center of the crystal of 84 K.

Possible thermal lens can now be calculated for the STP Ti:Sa crystal presented in Figure 1b. The temperature parabolic distribution presented by formula (5) was used as well, for the Y axis. Therefore, the modified formula for the focal distance calculation can be utilized [22]:

$$f = \frac{(Y/2)^2}{2OPD\left(\frac{Y}{2}\right)}, \tag{7}$$

where $OPD(Y/2)$ is the optical path difference between coordinates $y = Y/2$ and $y = 0$. Consequently, the OPD can be calculated by subtracting optical paths (OPs) through the Z axis for the given Y coordinates

$$OPD(\frac{Y}{2}) = \left[\frac{\partial n}{\partial T}\right] \int_0^Z (\Delta T\left(z, \frac{Y}{2}\right) - \Delta T(z, 0))dz. \tag{8}$$

The crystal dimension Y was taken from Figure 1b. The OP of the coordinate y was calculated by integrating the formula: $dOP(z, h) = \left[\frac{\partial n}{\partial T}\right]\Delta T(z, h)dz$ where ΔT is taken from the formula (5) and $\partial n/\partial T$ is supposed to be constant within the used temperature range. After integration, one can obtain: $OPD\left(\frac{Y}{2}\right) = \left[\frac{\partial n}{\partial T}\right]\frac{Q}{12K}Z^3$. It can be converted to $OPD\left(\frac{Y}{2}\right) = \left[\frac{\partial n}{\partial T}\right]\frac{R}{AK}Z$ by replacing Q with the heating density of the stress fracture limit from formula (3) and reducing it by factor A. Hence, replacing OPD in (7) we obtain:

$$f = \frac{AK(Y/2)^2}{2\left[\frac{\partial n}{\partial T}\right]RZ}. \tag{9}$$

The crystal size Y can be taken as equal to 1 cm, for certainty. The results of the focal distance dependence on the crystal thickness Z for different factors A can be seen in Figure 3.

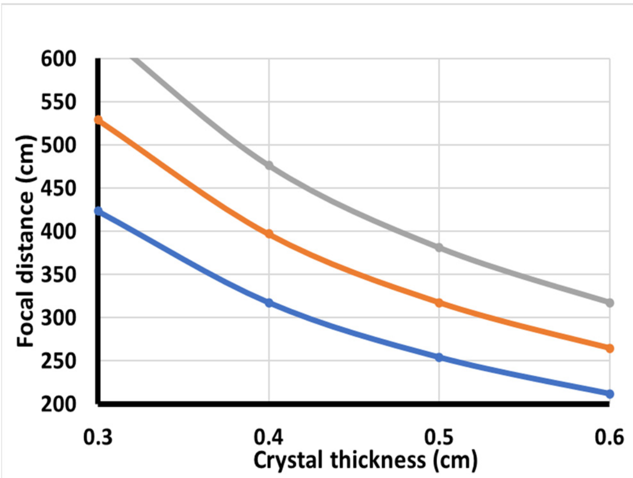

Figure 3. Focal distance on the crystal thickness (cm) for the different A factors (max. crystal temperature difference: 4 (125 K)—blue curve; 5 (100 K)—orange curve; 6 (85 K)—gray curve.

Here, the blue, orange, and gray curves also equaled the generated heat density of four, five, and six times below the stress fracture limit. From these results, one can conclude that the thermal lens focal lengths changed from 2 to 6 m for different heating densities and crystal thicknesses, which can be compensated for by using an appropriate radius of spherical mirrors of the amplifier optical scheme, as was done in [18] (see below for details).

3. Repetition Rate vs. Pump Energy

Now, utilizing the results of the previous chapter, the estimation of the maximal repetition rate dependence on the pump fluence can be carried out. The STP Ti:Sa crystal presented in Figure 1b was used for the above-discussed crystal thicknesses, and the temperatures from 85 to 125 °C that were used for the thermolens calculations were taken into account. Heat density can be presented as a fraction of the pump energy density multiplied by the repetition rate and can be used for the RR calculation:

$$RR = \frac{QZ}{kI}, \text{ using formula (3) } RR = \frac{12R}{kIAZ} \tag{10}$$

where I is the absorbed pump fluence in (J/cm^2) and k is the factor of total absorbed pump energy converted into the crystal heating, which is ~0.4 for Ti:Sa, and Z is the crystal thickness. The result of the calculation is presented in Figure 4. As seen from these curves, the pump fluence between 2 and 3 J/cm^2 (the crystal pumped through both sides) was possible when the RR was limited by a few hundred Hz. The calculation of the amplification process using the Frantz–Nodvik equation [23] allowed us to find the number of passes required to reach the effective output fluence over 1–1.5 J/cm^2. The classical butterfly-type optical scheme of the amplifier (Figure 1a) was used with the conventional TD or STP crystal shape, where the seed beam filled the full aperture of crystal. The results of the calculations are presented in Figure 5a. As seen, the required output fluence could be reached after three passes of the seed with the input fluence starting from 20 mJ/cm^2. Thus, the TD Ti:Sa crystal with a thickness of 4–5 mm and a diameter of 35 mm demonstrated a consistent performance using in an amplifier of 10 J the output energy. Technology for producing the Ti:Sa crystals with similar parameters is now available, and has already been employed; see, for example, [14].

The higher RR requires a lower pump fluence. For instance, in the case of the crystal temperature staying below 100° C and the repetition rate in the variety of 1–3 kHz, the pump fluence was in the range of 0.5–1 J/cm^2 (gray and orange curves of Figure 4b). As a result, the seed output fluence was than 0.6 J/cm^2 due to the quantum defect, and the energy extraction of a few Joules required a crystal aperture area of several tens of cm^2. TD or STP crystal shapes, where the pump and seed beams fill the full crystal aperture, leads to a poor energy extraction and, consequently, to a large number of seed passes. The final amplifier with an energy above 3 J is required for CPA Ti:Sa laser systems with an output power over 100 TW, assuming the compressor passes through an efficiency of 70% and the output pulse duration is 20 fs, which are the conventional parameters to date. A crystal with a pumping area above 6 cm^2 is needed, taking into account the reachable output fluence of 0.6 J/cm^2.

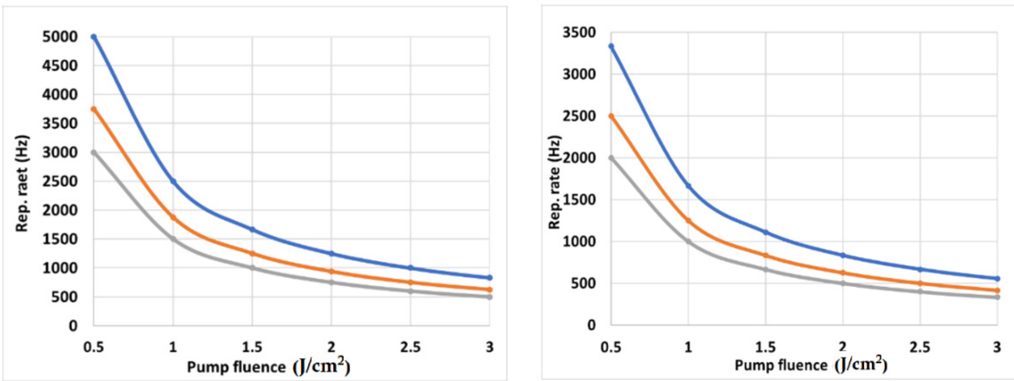

(**a**) (**b**)

Figure 4. The repetition rate (Hz) on absorbed pump fluence (J/cm^2): (**a**) the generated heat density of four times below the stress fracture limit; (**b**) six times below the stress fracture limit; crystals thickness: 0.3 cm—blue, 0.4 cm—orange, and 0.5 cm—gray.

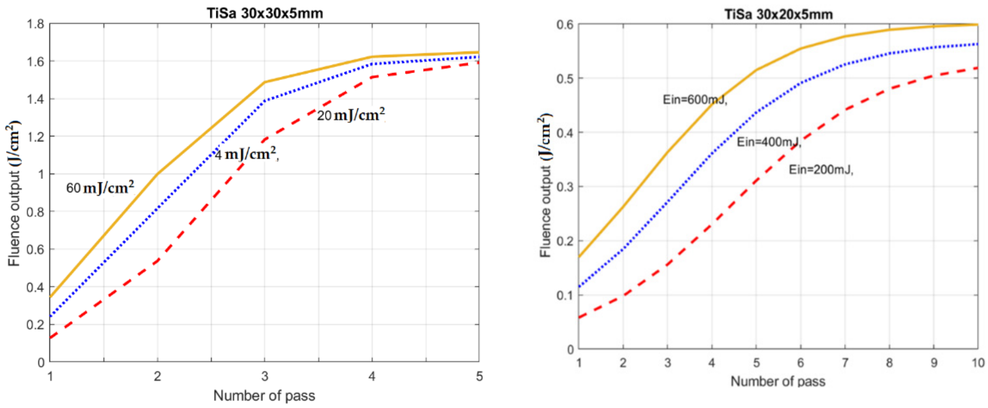

(**a**) (**b**)

Figure 5. Dependence of the output seed fluence on the number of passes through the crystal with the butterfly-type optical scheme of the amplifier for three different input seed fluences (energy): (**a**) pump fluence 3 J/cm^2, RR is below 1 kHz; (**b**) pump fluence 1 J/cm^2, RR above 1 kHz.

A pump energy up to 6 J per pulse in the green range of the wavelength with a 1 kHz repetition rate or higher is necessary for the pumping of this amplifier. The Yb:YAG laser with the second harmonic generation, which can deliver more than 1 J per pulse at 515 nm wavelength and the repetition rate of 1 kHz was demonstrated in [12]. The possibility of scaling this system up to 8 J was shown in [24].

The similar calculation that was made above was also applied for this amplifier. The results of these calculations are presented in Figure 5b.

As seen from this graph, the fluence of 0.6 J/cm^2 could be achieved after 10 passes through the crystal, when the input seed energy was 0.6 J (fluence of 0.1 J/cm^2). The size of each of the ten mirrors should be more than 2″, which leads to a distance of 2 m between the crystal and the mirrors to prevent the significant walk out of the seed from the pumped area. The total length of the optical scheme became greater than 4 m to keep reasonable angles between passes. In addition to the inconvenience of the very big footprint of the amplifier, the overall time of the seed traveling through the optical scheme was about 120 ns, which led to a considerable reduction in the stored energy due to ASE.

The alternative scheme and RTCP crystal geometry of the amplifier is presented in the Figure 6a, where only part of the crystal aperture was filling per pass. A similar scheme was suggested in [3,15] and tested in [18] with an XTS amplifier. The cross-section area of the seed beam was reduced to 2 × 1 cm^2, which allowed for increasing the fluence and, hence, the extraction efficiency.

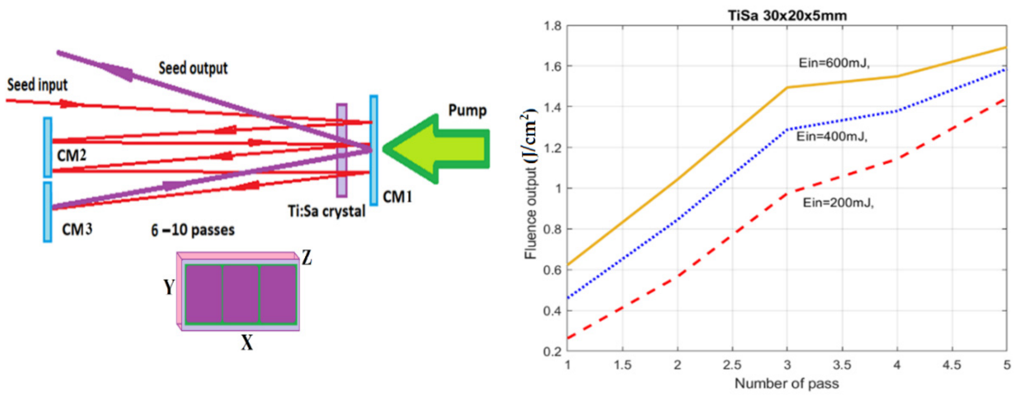

(**a**) (**b**)

Figure 6. (**a**) Optical scheme of the amplifier with RTCP Ti:Sa crystal geometry for a high RR; (**b**) dependence of the output seed fluence on the number of passes for three different input seed energies.

The optical scheme consists only of the three mirrors for the four to five seed double-passes through the Ti:Sa amplifier, as presented in Figure 6a (only four passes are shown for simplicity's sake). The seed beam can be relay imaged from pass to pass using curved mirrors (CM1–CM3), with a radius of curvature required to compensate for the thermolens. The Ti:Sa crystal was pumped through one or two large faces by one (as shown in Figure 6a) or two counter-propagating pump beams. The size of each of the three mirrors was below 3″, and the distance of 1–2 m between the crystal and the mirrors was enough to keep the acceptable angles between passes. Therefore, the presented scheme looks preferable due to its compactness and the small overall time required for the seed to travel through the optical scheme, which was about 30 ns in this case. It is also important to estimate the efficiency of the amplification of this scheme.

The results of this calculation are presented in Figure 6b. The output fluences were significantly higher, as can be expected, compared with the curves in Figure 5b for any passes (stages of amplification), and the required output energy of 3 J could be achieved even with 200 mJ of the input seed energy. The number of seed passes was reduced in the case of the higher input energy, for example, down to four double passes with 400 mJ of the input. Therefore, this optical scheme of the discussed amplifier is preferable due to its ability to achieve an RR above 1 kHz and the output energy of several Joules from the point of the energy extracting ability, as well as its better adaptiveness and compactness.

4. Conclusions

The dependence of pulse energy on the RR for the final amplifiers of CPA laser systems with different parameters was discussed in this paper. The necessity of using crystals with different geometries was demonstrated on the basis of the presented calculations. The chart of the required output average power dependence on the RR with preferable areas of usage for TD, RTCP, and XTS Ti:Sa crystal configurations is presented in Figure 7. As seen from this chart, the TD crystal could be used for the systems with an RR below a few hundred Hz if an output pulse energy above 10 s Joules was required (red area). The RTCP geometry was more suitable for Ti:Sa amplifiers with an RR above 1 kHz and an energy range of 0.1–10 J (violet area). Furthermore, the XTS crystal shape was more desirable for the amplifiers with a high RR above 1 kHz but with a low energy per pulse below 100 mJ (blue area) [15,18].

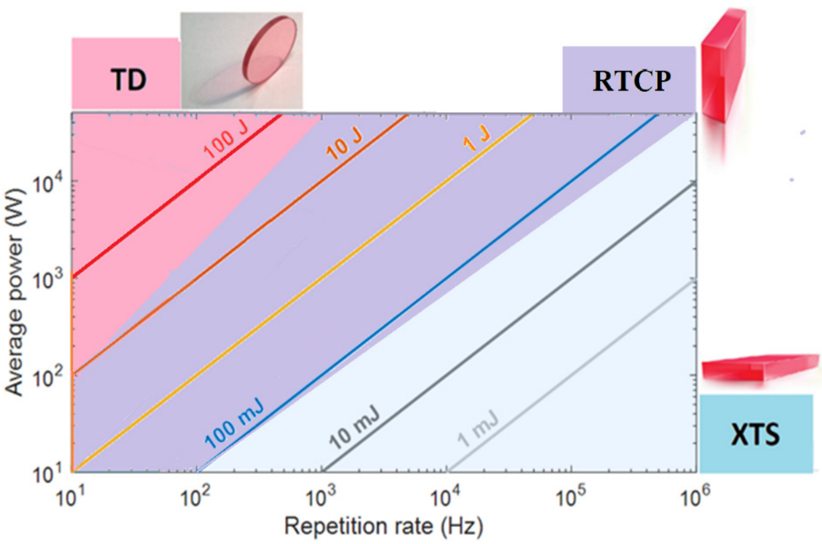

Figure 7. Output average power dependence on the RR with preferable areas of TD, RTCP, and XTS Ti:Sa crystal configurations.

Additionally, the possibility of building an RTCP Ti:Sa amplifier with more than 3 J of output energy and a repetition rate higher than 1 kHz for 100 s TW laser systems was discussed. The limitations placed by the crystal overheating were estimated and considered as a key restrictive factor for the output laser parameters. The acceptable pump fluence of Ti:Sa amplifiers was calculated. The evaluations of the thermolens developed by the pump heating for a crystal thickness of 3–6 mm and the maximal temperature around 100 °C were made. Finally, the optimal optical scheme of the RTCP amplifier was evaluated, and its ability to achieve the required output energy was estimated.

Funding: This research received no external funding.

Institutional Review Board Statement: Not applicable.

Informed Consent Statement: Not applicable.

Data Availability Statement: Not applicable.

Conflicts of Interest: The authors declare no conflict of interest.

References

1. Damm, T.; Kaschke, M.; Noack, F.; Wilhelmi, B. Compression of picosecond pulses from a solid-state laser using self-phase modulation in graded-index fibers. *Opt. Lett.* **1985**, *10*, 176. [CrossRef] [PubMed]
2. Strickland, D.; Mourou, G. Compression of amplified chirped optical pulses. *Opt. Commun.* **1985**, *56*, 219. [CrossRef]
3. Chvykov, V. Ti: Sa Crystals in Ultra-High Peak and Average Power Laser Systems. *Crystals* **2021**, *11*, 841. [CrossRef]
4. Chvykov, V.; Yanovsky, V.; Bahk, S.W.; Kalintchenko, G.; Mourou, G. Suppression of parasitic lasing in multi-pass Ti-sapphire amplifiers. In Proceedings of the Conference on Lasers and Electro-Optics, Baltimore, MD, USA, 1–6 June 2003.
5. Chvykov, V.; Krushelnik, K. Transverse amplified spontaneous emission: The limiting factor for output energy of ultra-high power lasers. *Opt. Commun.* **2014**, *312*, 216. [CrossRef]
6. Li, W.; Gan, Z.; Yu, L.; Wang, C.; Liu, Y.; Guo, Z.; Xu, L.; Xu, M.; Hang, Y.; Xu, Y.; et al. 339 J high-energy Ti:sapphire chirped-pulse amplifier for 10 PW laser facility. *Opt. Lett.* **2018**, *43*, 5681–5684. [CrossRef] [PubMed]
7. Yoon, J.W.; Kim, Y.G.; Choi, I.W.; Sung, J.H.; Lee, H.W.; Lee, S.K.; Nam, C.H. Realization of laser intensity over 1023 W/cm^2. *Optica* **2021**, *8*, 630–635. [CrossRef]
8. Mourou, G.A.; Tajima, T.; Bulanov, S.V. Optics in the relativistic regime. *Rev. Mod. Phys.* **2006**, *78*, 309. [CrossRef]
9. Rockwood, A.; Wang, Y.; Wang, S.; Berrill, M.; Shlyaptsev, V.N.; Rocca, J.J. Compact gain-saturated x-ray lasers down to 6.85 nm and amplification down to 5.85 nm. *Optica* **2018**, *5*, 257–262. [CrossRef]
10. Apollonov, V.V. High power disk laser. *Nat. Sci.* **2013**, *5*, 556–562. [CrossRef]
11. Tümmler, J.; Jung, R.; Stiel, H.; Nickles, P.V.; Sandner, W. High-repetition-rate chirped-pulse-amplification thin-disk laser system with joule-level pulse energy. *Opt. Lett.* **2009**, *34*, 1378–1380. [CrossRef] [PubMed]
12. Chi, H.; Wang, Y.; Davenport, A.; Menoni, C.S.; Rocca, J.J. Demonstration of a kilowatt average power, 1 J, green laser. *Opt. Lett.* **2020**, *45*, 6803–6806. [CrossRef] [PubMed]
13. Chvykov, V.; Nagymihaly, R.S.; Cao, H.; Kalashnikov, M.; Osvay, K. Design of a thin disk amplifier with extraction during pumping for high peak and average power Ti: Sa systems (EDP-TD). *Opt. Express* **2016**, *24*, 3721. [CrossRef] [PubMed]
14. Chvykov, V.; Cao, H.; Nagymihaly, R.; Kalashnikov, M.P.; Khodakovskiy, N.; Glassock, R.; Ehrentraut, L.; Schnuerer, M.; Osvay, K. High peak and average power Ti: Sapphire thin disk amplifier with extraction during pumping. *Opt. Lett.* **2016**, *41*, 3017. [CrossRef] [PubMed]
15. Cao, H.; Nagymihaly, R.S.; Chvykov, V. Cross thin slab kW-class Ti: Sapphire amplifiers. *Laser Phys.* **2019**, *29*, 065802. [CrossRef]
16. Russbueldt, P.; Mans, T.; Rotarius, G.; Weitenberg, J.; Hoffmann, H.D.; Poprawe, R. 400 W Yb: YAG Innoslab fs-amplifier. *Opt. Express* **2009**, *17*, 12230–12245. [CrossRef] [PubMed]
17. Russbueldt, P.; Mans, T.; Weitenberg, J.; Hoffmann, H.D.; Poprawe, R. Compact diode-pumped 1.1 kW Yb: YAG Innoslab femtosecond amplifier. *Opt. Lett.* **2010**, *35*, 4169–4171. [CrossRef] [PubMed]
18. Chvykov, V.; Chi, H.; Wang, Y.; Dehne, K.; Berrill, M.; Rocca, J.J. Demonstration of a side-pumped cross-seeded thin-slab pre-amplifier for high-power Ti:Sa laser systems. *Opt. Lett.* **2022**, *47*, 3463. [CrossRef] [PubMed]
19. Eggleston, J.; Kane, T.; Kuhn, K.; Unternahrer, J.; Byer, R. The Slab Geometry Laser-Part I: Theory. *IEEE J. Quantum Electron.* **1984**, *20*, 289–301. [CrossRef]
20. Koechner, W. *Solid-State Laser Engineering*; Springer: Berlin, Germany, 2013; Volume 1.
21. Available online: https://gtat.com/wp-content/uploads/2020/09/Ti-sapphire-Data-Sheet-0420.pdf (accessed on 1 September 2020).
22. Pfistner, C.; Weber, R.; Weber, H.P.; Merazzi, S.; Gruber, R. Thermal beam distortions in end pumped Nd: YAG, Nd: GSGG, and Nd: YLF rods. *IEEE J. Quantum Electron.* **1994**, *30*, 1605–1615. [CrossRef]
23. Frantz, L.M.; Nodvik, J.S. Theory of Pulse Propagation in a Laser Amplifier. *J. Appl. Phys.* **1963**, *34*, 2346. [CrossRef]
24. Laser technology for k-BELLA and beyond Workshop. In *Report of Workshop*; 21 Lawrence Berkeley National Laboratory: Berkeley, CA, USA, 2017.